

# Silicon-on-insulator waveguide photodetector with Ge/Si self-assembled islands

M. El kurdi, P. Boucaud,<sup>a)</sup> S. Sauvage, and G. Fishman

*Institut d'Électronique Fondamentale, UMR CNRS 8622, Bâtiment 220, Université Paris-Sud, 91405 Orsay, France*

O. Kermarrec, Y. Campidelli, and D. Bensahel

*STMICROELECTRONICS 850 Rue Jean Monnet, 38926 Crolles Cedex, France*

G. Saint-Girons, I. Sagnes, and G. Patriarche

*Laboratoire de Photonique et Nanostructures, Route de Nozay, 91406 Marcoussis, France*

(Received 1 April 2002; accepted for publication 22 May 2002)

We have investigated a silicon-based near-infrared photodetector using a waveguide with strong optical confinement. The high-difference index waveguide is obtained with a silicon-on-insulator substrate. The optically active region consists of self-assembled Ge/Si islands embedded in a *p-i-n* junction. The Ge/Si islands grown by high-pressure chemical-vapor deposition exhibit a broad photoluminescence and electroluminescence which are resonant around 1.5  $\mu\text{m}$ . The photoluminescence and electroluminescence energies are correlated to the island size and to the island composition using a six-band  $\mathbf{k}\cdot\mathbf{p}$  calculation. The spectral responsivity of the detectors is measured in a front facet coupling geometry with a broadband source and with semiconductor laser diodes. For a 0 V applied bias, responsivities of 25 and 0.25 mA/W are measured at room temperature at 1.3 and 1.55  $\mu\text{m}$ , respectively. © 2002 American Institute of Physics.

[DOI: 10.1063/1.1493656]

## I. INTRODUCTION

Silicon-on-insulator substrates offer opportunities for integrated optics and microphotonic applications.<sup>1</sup> A thick buried oxide covered by a crystalline silicon layer leads to a very high difference of refractive index, with a difference  $\Delta n$  as large as two in the near-infrared spectral range. With such a large variation, strong optical confinement can be easily achieved in the transparency window of silicon, and in particular, in the spectral windows around 1.3 and 1.55  $\mu\text{m}$  corresponding to the telecommunication wavelengths.<sup>2</sup> Silicon-on-insulator substrates open the route to integrated optics at a reduced scale with microwaveguides, bends, and couplers, while keeping the compatibility with the standard silicon fabrication techniques. To achieve a high degree of integration, active components like optical sources or photodiodes that can be coupled to this technology are required. The hybridization of III-V semiconductor components represents one possibility. Another route relies on IV-IV heterostructures epitaxially grown on silicon. As compared to silica-on-silicon platforms, silicon-on-insulators substrates offer the advantage of epitaxial regrowth. It has been demonstrated that Ge/Si self-assembled islands with their high-germanium content are good candidates to operate at telecommunication wavelengths.<sup>3</sup> Moreover, the Ge/Si self-assembled islands which emit and absorb light at 1.3–1.55  $\mu\text{m}$  can be epitaxially covered by silicon and offer the advantage of silicon-terminated surfaces, thus keeping the compatibility with silicon standard processing.

In this article, we report on silicon-on-insulator waveguide photodetectors with Ge/Si self-assembled islands embedded in a *p-i-n* junction. A structural and an optical analysis of the devices are presented. The emission wavelength of the islands is correlated to the structural parameters and to the emission energy obtained in the framework of a six-band  $\mathbf{k}\cdot\mathbf{p}$  calculation. The responsivity of the device is measured at 1.3 and at 1.55  $\mu\text{m}$  wavelengths.

## II. EXPERIMENTAL DETAILS

The self-assembled quantum dots were grown in an industrial lamp-heated single wafer chemical-vapor deposition reactor on 200-mm-diameter (001) oriented silicon-on-insulator substrates. Silane and germane diluted in hydrogen carrier gas were used as gas precursors. The process temperature deposition was around 700 °C, at a total pressure lower than 100 Torr.<sup>4</sup> Starting from the silicon substrate, it consists of a 0.4- $\mu\text{m}$ -thick oxide layer, a 0.15- $\mu\text{m}$ -thick Si layer, a 0.2- $\mu\text{m}$ -thick  $p^+$  Si layer *in situ* doped with boron ( $10^{19}\text{ cm}^{-3}$ ) using  $\text{B}_2\text{H}_6$  diluted in  $\text{H}_2$ , a 30-nm-thick Si spacer layer, five self-assembled quantum island layers separated by 65-nm-thick Si barrier layers, and a 100-nm-thick  $n^+$  contact layer *in situ* doped with phosphine diluted in  $\text{H}_2$  ( $10^{19}\text{ cm}^{-3}$ ). A schematic diagram of the structure appears in Fig. 1(a). The detectors were processed by reactive ion etching into 100- $\mu\text{m}$ -large ridge waveguides. The etch depth was 0.4  $\mu\text{m}$ . Devices with lengths going from 3 to 7 mm were measured. The ohmic contacts with the  $p^+$  and the  $n^+$  layers were obtained by depositing Ti/Au contacts. The detectors

<sup>a)</sup>Electronic mail: philippe.boucaud@ief.u-psud.fr

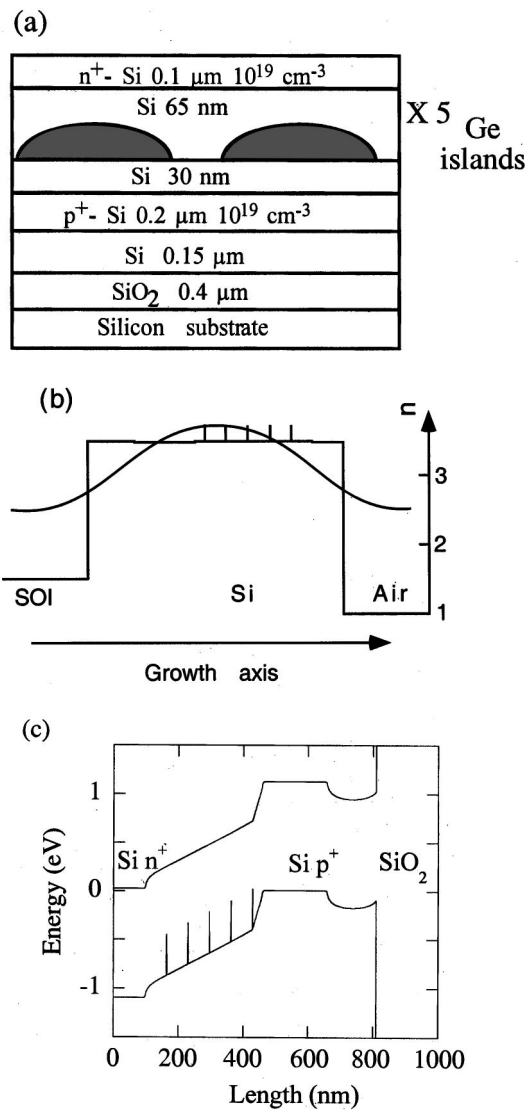


FIG. 1. (a) Schematic diagram of the device structure showing the vertical stacking of the layers (not to scale). (b) Index variation along the  $z$  direction for the silicon-on-insulator structure. The profile of the first confined optical mode in TE polarization at  $1.3 \mu\text{m}$  is superimposed on the index variation. The island layers appear as five spikes. (c) Band structure of the device for a 0 V applied bias.

were glued to a ceramic pedestal. The top and back contacts were bonded with gold wires using standard thermocompression bonding.

Figure 1(b) shows the calculated profile of the fundamental confined optical mode in transverse-electric (TE) polarization at  $1.3 \mu\text{m}$ . The calculation was performed without accounting of the ridge waveguide etching. The refractive index of the doped layers was taken from Ref. 5. A strong confinement of the optical waves along the  $z$  direction is observed in this structure with a large refractive-index difference ( $n_{\text{SiO}_2} \sim 1.46$  and  $n_{\text{Si}} \sim 3.5$ ).<sup>6</sup> This refractive-index difference of  $\sim 2$  is significantly larger than the one that can be achieved with pseudomorphic  $\text{Si}_{1-x}\text{Ge}_x$  waveguides.<sup>1</sup> In the investigated structure, the total thickness above the buried oxide layer is  $\sim 0.80 \mu\text{m}$ . This large thickness does not allow a single-mode propagation. Four optical modes are confined

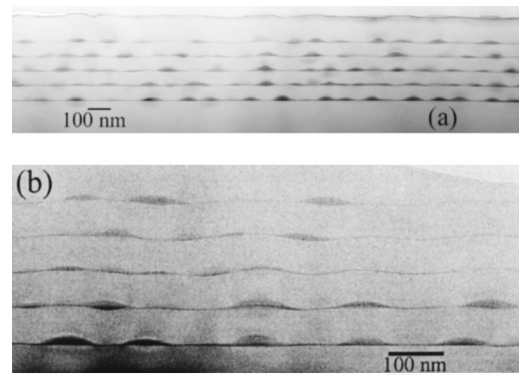


FIG. 2. (a) Cross-section transmission electronic microscopy image of a sample grown in the same conditions as the processed samples. The lateral size of the image is  $2.24 \mu\text{m}$  and the height is  $560 \text{ nm}$ . The image is taken in bright-field condition along the  $[004]$  direction. The islands and the wetting layers appear in dark contrast. (b) Cross-section image at a higher magnification. The image lateral size is  $930 \text{ nm}$ .

along the  $z$  direction in both TE and TM (transverse-magnetic) polarizations at  $1.3 \mu\text{m}$ . At  $1.55 \mu\text{m}$ , four (three) modes are confined in TE (TM) polarizations. The calculated band alignment of the structure at 0 V applied bias is shown in Fig. 1(c).

### III. RESULTS

Figure 2(a) shows a cross-section transmission electronic microscopy image of a waveguide structure grown in the same condition as the processed sample but without the doped layers. The self-assembled islands and the wetting layers appear in dark contrast as a consequence of the bright-field imaging conditions along the  $[004]$  direction. The dot density is around  $3 \times 10^9 \text{ cm}^{-2}$ . The islands in the first layer have a dome-shaped geometry. A bimodal distribution is observed with an average island in-plane size of  $85 \text{ nm}$  and average heights of  $11$  and  $17 \text{ nm}$ . Figure 2(b) shows a cross-section image at a higher magnification. No vertical ordering from layer to layer is observed. The thickness of the silicon capping layer is not large enough to flatten the surface and the large buried islands lead to surface undulations in the successive layers. The islands preferentially nucleate in the depression region, on the edges of the undulations, close to the island top leading to an oblique stacking.<sup>7</sup> Separate measurements on single islands have shown that the average Ge content of the buried self-assembled islands grown in similar conditions at a temperature of  $650 \text{ }^\circ\text{C}$  is around  $50\%$ .<sup>8</sup>

Figure 3 shows the low-temperature (5 K) photoluminescence and the electroluminescence spectra of the self-assembled islands measured at  $80 \text{ K}$ . The photoluminescence was excited with an  $\text{Ar}^+$  ion laser. For the electroluminescence measurements, the light was collected through the cleaved facet of the device. Luminescence spectra are known to provide valuable information on the self-assembled islands. We note that self-assembled islands embedded in a waveguide structure with a strong optical confinement can be used as an integrated optical probe of the waveguides. In the present case, no difference is observed between the luminescence spectra in the waveguide structure and in standard

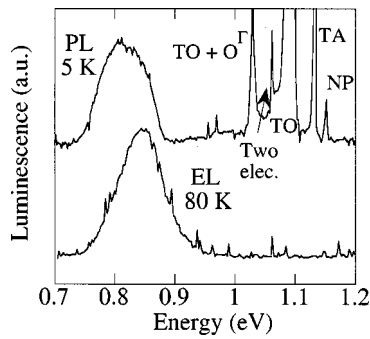


FIG. 3. 5 K photoluminescence (top figure) and 80 K electroluminescence (bottom figure). The driving current for the electroluminescence is  $12 \text{ A cm}^{-2}$ . The recombination associated with the self-assembled islands is resonant around 0.8 eV. The Si-related recombination lines correspond to the no-phonon (NP), transverse-acoustic phonon (TA), transverse-optical phonon (TO), two-electron and one transverse-optical phonon (two elec.) and two-phonon ( $\text{TO} + \text{O}_T$ ) recombinations.

multilayer structures since the thickness of the waveguide is too large for single-mode operation at these wavelengths. At low temperature, recombination lines associated with the bulk silicon are observed at energies larger than 1 eV. They correspond to the no-phonon (1.152 eV), acoustic phonon-assisted (1.133 eV), transverse-optical phonon (1.094 eV), two-electron and one transverse-optical phonon (1.06 eV), and two-phonon (band edge + zone center at 1.03 eV) exciton recombinations.<sup>9</sup> Both photoluminescence and electroluminescence spectra exhibit a large resonance at low energy with a maximum around 0.815 eV ( $1.52 \mu\text{m}$ ) for the photoluminescence and 0.845 eV ( $1.47 \mu\text{m}$ ) for the electroluminescence. These large resonances with a 95 meV broadening are attributed to the optical recombination of the carriers in the self-assembled layers.<sup>10</sup> The energy difference between both spectra results from the temperature difference and from the difference of polarization and carrier densities.<sup>11</sup> The electronic structure of the islands was obtained using a quantum well calculation in the six-band  $\mathbf{k}\cdot\mathbf{p}$  framework.<sup>12</sup> The islands are approximated by an equivalent two-dimensional SiGe layer with a 50% Ge content and thicknesses of 11 and 17 nm. The strain field in the island was taken constant and equivalent to the one of a tetragonally strained SiGe layer. This assumption is consistent with electronic-diffraction measurements performed on similar structures grown at a lower temperature.<sup>8</sup> For a pseudomorphic tetragonal deformation, the band offset occurs mainly in the valence band, with a negligible contribution in the conduction band. At low temperature, the energy gap of a pseudomorphic compressively strained  $\text{Si}_{0.5}\text{Ge}_{0.5}$  alloy is  $\sim 0.8 \text{ eV}$ .<sup>13</sup> The confinement energy at the center of the Brillouin zone of the first heavy-hole subband is 58, 30, 18, 10, and 5 meV for a 4, 6, 8, 11, and 17 nm thick layer, respectively. The photoluminescence energy is thus expected at  $\sim 0.81 \text{ eV}$  if we consider an average equivalent height of 11 nm, in satisfying agreement with the experimental photoluminescence data. Band-filling effects are not considered in this estimation.<sup>11</sup> We emphasize that this calculation, valid for a two-dimensional approximation, only accounts for a uniform strain distribution. The strain relaxation within the islands can lead to a tensile-

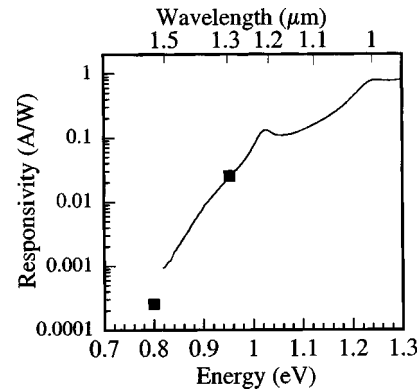


FIG. 4. Responsivity of the device measured at room temperature with a 0 V applied bias. The full curve corresponds to a calibrated measurement with a Fourier-transform infrared spectrometer. The squares correspond to measurements at  $1.3 \mu\text{m}$  (0.953 eV) and  $1.55 \mu\text{m}$  (0.8 eV) with laser diodes.

strained silicon surrounding the islands, which lowers the energy gap.<sup>14</sup> A full calculation accounting for the strain-field variation and the three-dimensional geometry of the island is beyond the scope of this article. It is obvious that the composition and the strain fields are the key features governing the photoluminescence energy, while the confinement energy has a smaller contribution.

Figure 4 shows the spectral responsivity of the devices measured in a front facet coupling geometry. The spectral response of the devices was measured with a microscope coupled to a Fourier-transform infrared spectrometer and with continuous-wave semiconductor laser diodes at 1.3 and  $1.55 \mu\text{m}$ . In the latter case, the laser was focused with a  $3 \mu\text{m}$  spot diameter using optics with a 0.6 numerical aperture. The measurement was performed at room temperature with a 0 V applied bias on a 7-mm-long device. No difference was observed between 3- and 7-mm-long devices. The calibrated response does not account for the coupling efficiency into the waveguide. The reported values represent therefore lower values of the responsivity. The weak-coupling efficiency also explains that the response is below the noise level at  $1.55 \mu\text{m}$  with the Fourier-transform spectrometer. It can however be easily measured with a laser diode. At high energy, two small resonances are observed at 1.026 and 1.25 eV. The energy spacing between these resonances corresponds to the periodicity of the Fabry–Perot resonances measured at normal incidence. A responsivity of 25 and 0.25 mA/W are measured at 1.3 and  $1.55 \mu\text{m}$ . We did not observe any significant difference between TE- and TM-polarized excitations at  $1.55 \mu\text{m}$ . For a 0 V applied bias, the responsivity decreases by two orders of magnitude between 1.3 and  $1.55 \mu\text{m}$ . This roll off stems from the absorption decrease at long wavelength but also from the carrier trapping by the potential barriers in the valence band and from a low-escape probability of the holes, as illustrated in Fig. 1(b).

#### IV. DISCUSSION

These measurements show that photodetectors with Ge/Si self-assembled islands embedded in a silicon–on–insulator waveguide can be operated at the telecommunication wavelengths of 1.3 and  $1.55 \mu\text{m}$ . At  $1.55 \mu\text{m}$ , the re-

sponsivity of the device remains lower than the one reported for pure Ge layers,<sup>15</sup> for metal–semiconductor–metal structures with Si<sub>0.5</sub>Ge<sub>0.5</sub> undulating layers,<sup>16</sup> or III–V devices. The external quantum efficiency of the investigated device deduced from the responsivity for a 0 V applied bias is 2.35% at 1.3  $\mu\text{m}$  and 0.02% at 1.55  $\mu\text{m}$ . One advantage of Ge/Si self-assembled islands is to avoid the presence of Ge terminated surfaces, thus keeping the compatibility with the silicon fabrication techniques. We note that the present responsivities are not corrected for the coupling efficiency into the cleaved facet of the waveguide. The internal quantum efficiency at large wavelength is thus expected to be significantly enhanced as compared to the reported external quantum efficiency for a 0 V applied bias. A better coupling into this high-refractive-index difference waveguide could be achieved with appropriate tapers. Besides, a large reverse applied bias should increase the responsivity, by increasing the escape probability for the trapped carriers.<sup>17</sup> Separate measurements on devices containing self-assembled islands embedded in a SiGe 2% waveguide have shown an increase of the responsivity at low temperature by a factor of 4 for a reverse applied bias of 4 V. In the present device, the dark current at a high-reverse applied bias was too large. This dark current should be strongly reduced by a proper surface passivation after etching of the ridge waveguide. We note that absorption measurements performed on self-assembled islands embedded in a SiGe 2% waveguide have shown that the absorption roll off is around 1.9  $\mu\text{m}$ .<sup>3</sup> The decrease of the responsivity between 1.3 and 1.55  $\mu\text{m}$  is thus not associated with a significant absorption decrease.

## V. CONCLUSION

In conclusion, we have reported on near-infrared waveguide photodetectors using Ge/Si self-assembled islands. The islands were embedded into a silicon–on–insulator waveguide. The use of the silicon–on–insulator technology allows the achievement of waveguide with a strong optical

confinement, while keeping the compatibility with the silicon fabrication techniques. The photoresponse of the devices was measured at 1.3 and 1.55  $\mu\text{m}$ . At 1.3  $\mu\text{m}$ , a responsivity of 25 mA/W was obtained at room temperature under a 0 V applied bias in a front facet coupling geometry.

## ACKNOWLEDGMENT

This work was partly supported by the Réseau Micro et Nanotechnologie (RMNT) under Contract No. 00V0091.

- <sup>1</sup>B. Schüppert, J. Schmidtchen, A. Splett, U. Fischer, T. Zinke, R. Moosburger, and K. Petermann, *J. Lightwave Technol.* **14**, 2311 (1996).
- <sup>2</sup>R. A. Soref, J. Schmidtchen, and K. Petermann, *IEEE J. Quantum Electron.* **27**, 1971 (1991).
- <sup>3</sup>M. Elkurdi, P. Boucaud, S. Sauvage, O. Kermarrec, Y. Campidelli, D. Bensahel, G. Saint-Girons, and I. Sagnes, *Appl. Phys. Lett.* **80**, 509 (2002).
- <sup>4</sup>C. Hernandez, Y. Campidelli, D. Simon, D. Bensahel, I. Sagnes, G. Patriarache, P. Boucaud, and S. Sauvage, *J. Appl. Phys.* **86**, 1145 (1999).
- <sup>5</sup>R. A. Soref and B. R. Bennett, *IEEE J. Quantum Electron.* **23**, 123 (1987).
- <sup>6</sup>S. Janz, J. M. Baribeau, A. Delage, H. Lafontaine, S. Mailhot, R. L. Williams, D.-X. Xu, D. M. Bruce, P. E. Jessop, and M. Robillard, *IEEE J. Sel. Top. Quantum Electron.* **4**, 990 (1998).
- <sup>7</sup>P. Sutter, E. Mateeva-Sutter, and L. Vescan, *Appl. Phys. Lett.* **78**, 1736 (2001).
- <sup>8</sup>G. Patriarache, I. Sagnes, P. Boucaud, V. Le Thanh, D. Bouchier, C. Hernandez, Y. Campidelli, O. Kermarrec, and D. Bensahel, *Appl. Phys. Lett.* **77**, 370 (2000).
- <sup>9</sup>P. J. Dean, J. R. Haynes, and W. F. Flood, *Phys. Rev.* **161**, 711 (1967).
- <sup>10</sup>P. Schittenhelm, M. Gail, J. Brunner, J. F. Nützel, and G. Abstreiter, *Appl. Phys. Lett.* **67**, 1292 (1995).
- <sup>11</sup>P. Boucaud, S. Sauvage, M. Elkurdi, E. Mercier, T. Brunhes, V. Le Thanh, D. Bouchier, O. Kermarrec, Y. Campidelli, and D. Bensahel, *Phys. Rev. B* **64**, 155 310 (2001).
- <sup>12</sup>M. El kurdi, G. Fishman, S. Sauvage, and P. Boucaud (unpublished).
- <sup>13</sup>R. People, *IEEE J. Quantum Electron.* **22**, 1696 (1986).
- <sup>14</sup>O. G. Schmidt, K. Eberl, and Y. Rau, *Phys. Rev. B* **62**, 16 715 (2000).
- <sup>15</sup>L. Colace, G. Masini, G. Assanto, H. C. Luan, K. Wada, and L. C. Kimerling, *Appl. Phys. Lett.* **76**, 1231 (2000).
- <sup>16</sup>H. Lafontaine, N. L. Rowell, S. Janz, and D. X. Xu, *J. Appl. Phys.* **86**, 1287 (1999).
- <sup>17</sup>F. Y. Huang, X. Zhu, M. O. Tanner, and K. L. Wang, *Appl. Phys. Lett.* **67**, 566 (1995).